AGU PUBLICATIONS

Tectonics

RESEARCH ARTICLE
10.1002/2015TC003902

The Shillong Plateau and the great 1897 Assam earthquake

Philip England[1] and Roger Bilham[2]

[1]Department of Earth Sciences, University of Oxford, Oxford, UK, [2]Department of Geological Sciences, University of Colorado Boulder, Boulder, Colorado, USA

Key Points:
- Analysis of the Great 1897 earthquake with newly discovered triangulation data
- Confirms that the earthquake, M_w8.15-8.35, took place on the Oldham fault
- Oldham fault is one of several faults that pose seismic hazard to the region

Correspondence to:
P. England,
philip.england@earth.ox.ac.uk

Citation:
England, P., and R. Bilham (2015), The Shillong Plateau and the great 1897 Assam earthquake, *Tectonics*, *34*, doi:10.1002/2015TC003902.

Received 9 APR 2015
Accepted 29 JUL 2015
Accepted article online 3 AUG 2015

Abstract Previous analysis of triangulation data of the Survey of India concluded that the great 1897 Assam earthquake occurred on a south dipping fault near the northern edge of the Shillong Plateau, which was named the Oldham fault. This attribution has been questioned on geological and geodetic grounds. We refine the triangulation data, adding recently discovered observations, and demonstrate that they require average slip of 25 ± 5 m on a fault that dips south at ~40° beneath the plateau. The best fitting solution to the geodetic observations gives a rupture length of 79 km. However, the Chedrang fault, immediately to the west of the Oldham fault, appears to have slipped as a subvertical tear fault during or shortly after the 1897 earthquake, with over 10 m of down-to-the-west normal-sense slip. This observation suggests that the western end of the main rupture approached within a few kilometers of the Chedrang fault, giving a length of 95 km for the rupture. This range of parameters gives a magnitude $8.15 < M_w < 8.35$ for the earthquake. The triangulation data cannot be satisfied by slip on the north dipping faults that border the southern edge of the Shillong Plateau nor by slip on a south dipping fault that has been postulated in the Brahmaputra Valley. GPS velocities show that up to 5 mm/yr of shortening is taken up across the plateau and its borders; this suggests, via moment-frequency relations, that the interval between great earthquakes in the region is several thousand years but that earthquakes of magnitude 7 or greater should occur roughly once per century.

1. Introduction

The great earthquake of 12 June 1897 raised part of the northern edge of the Shillong Plateau by roughly 10 m but resulted in no primary surface rupture. We have previously [*Bilham and England*, 2001] analyzed this earthquake using angle changes derived from displacement vectors published for two geodetic networks: one crossing the plateau in the N-S direction [*Oldham*, 1899] and the other running E-W along the Brahmaputra valley to the north of the plateau [*Wilson*, 1938] (Figure 1). We determined that these observations implied slip on a blind south dipping reverse fault, close to the northern edge of the plateau, which we referred to as the Oldham fault.

This conclusion has subsequently been questioned. Some have followed the supposition of *Seeber and Armbruster* [1981] that the Dauki fault at the southern edge of the plateau slipped in the earthquake [*Morino et al.*, 2014] or have proposed the fresh-looking scarp of the Dauki fault, and that of the Dapsi fault to its west, as a contender for slip in 1897 [*Kali et al.*, 2013]. Others accept the notion of a south dipping blind thrust fault but, contending that morphological evidence for its presence in the northern plateau is weak, have conjectured an alternative location 50 km to the north, close to the Brahamaputra river [*Rajendran et al.*, 2004]; there are, however, compelling arguments to reject that conjecture [*Bilham*, 2006; *Sukhija et al.*, 2006]. The brevity of our original article precluded a comprehensive exposition of the geodetic data, and this shortfall has permitted much unnecessary speculation about the existence, location, and slip of the Oldham fault in the 1897 earthquake. This speculation is of obvious significance in the assessment of seismic hazard in the northeastern part of the Indian subcontinent. The attribution of an earthquake of magnitude greater than 8 to one fault (or nonexistent fault) has an impact upon assessment of hazard associated not only with that fault but also with other faults of the region.

The present article is motivated by a number of developments that throw additional light on these issues. First, a publication has been discovered [*Burrard*, 1898] that lists angle changes directly in the geodetic network on the hanging wall of the Oldham fault. Second, digital elevation data from the Shuttle Radar Topographic Mission (SRTM) [*Farr et al.*, 2007] and Google Earth images allow us to support the geodetic solution with

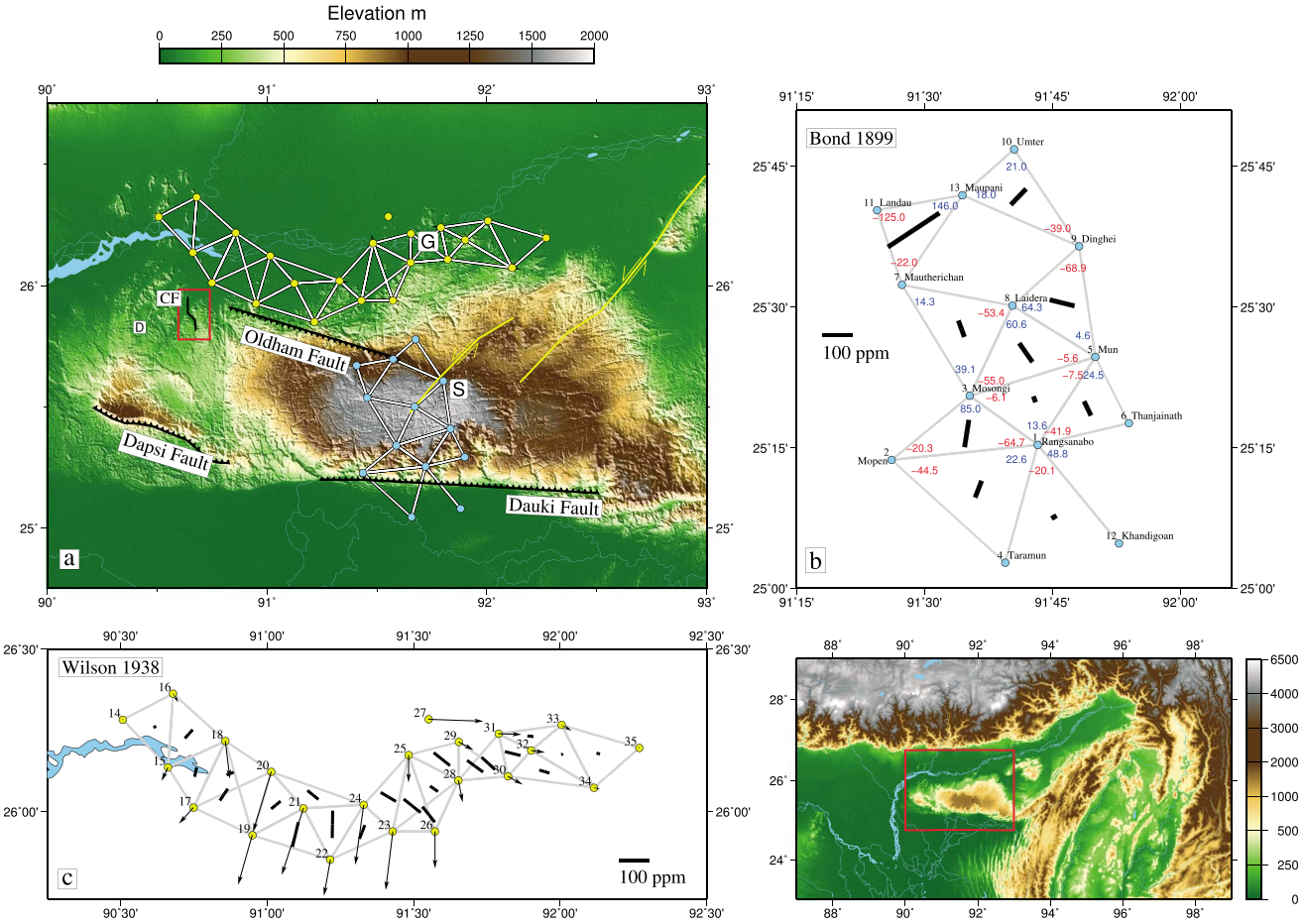

Figure 1. Setting and locations of triangulation networks. (a) Topography (scale to upper right) and locations of features discussed in the text. Major reverse faults are shown with teeth on the hanging wall; the Chedrang fault (CF, enclosed in red box marking location of Figure A1) is shown by a black line. Yellow lines with arrows show the locations of left-lateral strike-slip faults recorded by *Taylor and Yin* [2009]. Locations of the sites occupied by *Bond* [1899] and *Wilson* [1938] are shown, respectively, by blue and yellow dots. Single-letter labels show the cities of Guwahati (G) and Shillong (S) and the epicenter of the 1930 Dhubri earthquake (D). (b) Stations and angular changes measured by *Bond* [1899], as reported by *Burrard* [1898] (Tables 1 and 2). (c) Sites occupied by *Wilson* [1938]; numbers correspond to sites listed in Table 2, and triangles, implying angles observed, are taken from the figure in this report. Bars, scale to lower left, show the magnitude of Γ (equation (3)) and the orientation of the axis of maximum horizontal contraction (equation (4)) for each triangle and are plotted with their centers on the centroid of the relevant triangle.

geomorphological observations both on the Oldham fault and on the neighboring Chedrang fault. Third, recent geodetic determination of the rate of rotation of the Shillong Plateau relative to the Indian plate prompts a revised estimate of the rate of shortening across the faults bounding the Shillong Plateau. Finally, we take this opportunity to furnish future investigators with lists of raw data in the form of coordinates and angle changes, should they wish to test or build upon our findings.

2. The Triangulation Data

We constrain the rupture of the 1897 earthquake using four sets of trigonometrical observations: preseismic measurements from the Eastern Meridional series and Assam Valley series of the Great Trigonometrical Survey of India [*Strahan*, 1891; *Walker*, 1882] and postseismic surveys of these same points, undertaken at different times (Figure 1a). Immediately following the earthquake, R.D. Oldham persuaded Sydney Burrard, then Director General of the Survey of India, to resurvey points across the Shillong Plateau whose positions had been determined during surveys in the 1860s; this work was carried out by *Bond* [1899] (Figure 1b and Tables 1 and 2). Oldham also recommended remeasurement of a survey along the northern edge of the plateau, which eventually took place in 1936 [*Wilson*, 1938] (Figure 1c and Table 2).

Table 1. Angular Changes Measured by *Bond* [1899], as Reported by *Burrard*[1898][a]

Observing Station	Between		$\Delta\phi$ (arcsec)
1	4	2	4.67
1	2	3	−13.35
1	5	6	−8.64
1	3	5	2.80
1	4	12	−4.15
1	6	12	10.07
2	1	4	−9.18
2	1	3	−4.18
3	2	1	17.53
3	1	5	−1.26
3	5	8	−11.34
3	8	7	8.07
5	1	3	−1.54
5	1	6	5.05
5	3	8	−1.15
5	8	9	0.94
8	5	3	12.49
8	7	3	−11.02
8	9	5	13.27[b]
7	8	3	2.95
9	8	5	−14.21
10	13	9	4.33[c]
13	10	9	3.71 [a]
9	10	13	−8.05[a]
13	11	7	30.12[a]
11	13	7	−25.79[b]
7	11	13	−4.54[c]

[a]For each entry, the angle between the second and third stations was measured at the first station; station numbers refer to Table 2. $\Delta\phi$ is the angle measured in 1897–1898 minus the value of that angle determined in pre-earthquake surveys. Six angles not quoted by *Burrard* [1898] are derived from changes in line length given by *Oldham* [1899].
[b]Incorrectly printed as −13.27 in *Burrard* [1898].
[c]Derived from displacements listed by *Bond* [1899].

In Figure 1, we display the observations of Tables 1 and 2 in terms of the two components of shear strain:

$$\gamma_1 = \frac{\partial u_1}{\partial x_1} - \frac{\partial u_2}{\partial x_2}, \tag{1}$$

$$\gamma_2 = \frac{\partial u_1}{\partial x_2} + \frac{\partial u_2}{\partial x_1}, \tag{2}$$

where $u_{1,2}$ are components of displacement in the $x_{1,2}$ horizontal directions [*Frank*, 1966]. These shear strains, which are the only components of the strain tensor that may be determined from angle changes, may also be expressed in terms of the total shear strain

$$\Gamma = \sqrt{\gamma_1^2 + \gamma_2^2}, \tag{3}$$

and the orientation of one principal axis of horizontal strain; here we choose the azimuth of the most contractional (smaller positive or more negative) principal strain, whose azimuth ψ, measured clockwise from north, is given by

Table 2. The Locations of Triangulations Stations Occupied in the Resurveys Following the 1897 Assam Earthquake[a]

	Station	Longitude °E	Latitude °N	Displacement Up (m)	East (m)	North (m)
1	Rangsanabo	91.7216	25.2554	-		
2	Mopen	91.4357	25.2287	−1.2		
3	Mosongi	91.5887	25.3426	1.2		
4	Taramun Tila	91.6578	25.0456	2		
5	Mun	91.8343	25.4117	0.6		
6	Thanjainath	91.8995	25.2940	0.9		
7	Mautherichan	91.4561	25.5397	7.3		
8	Laidera	91.6718	25.5028	1.8		
9	Dinghei	91.8023	25.6081	2.1		
10	Umter	91.6753	25.7801	0.9		
11	Landau	91.4071	25.6721	5.2		
12	Khandigoan	91.8804	25.0802	1.9		
13	Maupani	91.5741	25.6988	-		
14	Bhairaber	90.5082	26.2835	1.2	0	0
15	Raikusni	90.6623	26.1365	1.5	−0.27	−0.56
16	Narikola	90.6798	26.3638	1.2	0.2	−0.37
17	Dabli	90.7495	26.0125	1.8	−0.6	−0.67
18	Bagbo	90.8583	26.2177	1.2	0.19	−3.57
19	Ghorkar	90.9504	25.9275	0.6	−0.59	−2.08
20	Nagarberha	91.0147	26.1230	0	−0.76	−2.5
21	Sonora	91.1245	26.0106	0	−0.91	−2.79
22	Langturi	91.2157	25.8519	0.3	−0.27	−3.51
23	Harogoan	91.4288	25.9394	0	−0.3	−2.45
24	Akchalia	91.3300	26.0215	−0.3	−0.35	−2.49
25	Hathimura	91.4828	26.1750	0	0	−3.14
26	Tepkilabama	91.5730	25.9395	−0.3	0	−3.54
27	Barambai	91.5513	26.285	0.3	2.3	−0.08
28	Maiang	91.6529	26.0966	0	0.18	−0.92
29	Sila	91.6543	26.2150	0.9	0.62	−0.34
30	Kurua	91.8223	26.1090	0	0.62	−0.34
31	Mairangka	91.7903	26.2400	0	0.96	−0.03
32	Parahopa	91.9013	26.1890	0	0.58	−0.08
33	Desh	92.0049	26.2672	0	0.41	−0.23
34	Dumria	92.1153	26.0740	0.3	0.25	−0.04
35	Tatalia	92.2702	26.1968	0	0	0

[a]The longitudes have been shifted by 0.0417° to the west, correcting a stated error in the station coordinates [*Walker*, 1882]. Stations 1–13 were occupied in 1897–1898 [*Bond*, 1899; *Burrard*, 1898; *Oldham*, 1899]. Stations 14–35 were occupied in 1936 by *Wilson* [1938]; displacements are read from Wilson's map (see text).

$$\sin(2\phi) = \frac{\gamma_2}{\Gamma}, \quad \cos(2\phi) = -\frac{\gamma_1}{\Gamma} \quad \psi = \phi + \frac{\pi}{2} \tag{4}$$

(*Savage and Burford* [1970], correcting *Frank* [1966]).

In addition to the horizontal angle changes of *Bond* [1899] and the calculated site displacements of *Wilson* [1938], Figure 1 also displays the shear strains, derived from these measurements, within triangles

Table 3. Height Changes at Subsidiary Stations Measured by *Bond* [1899], as Reported by *Oldham*[1899][a]

Station	Longitude °E	Latitude °N	Vertical (m)
Rableng	91.91	25.47	0.8
Shillong	91.84	25.53	1.3
Somullion	91.87	25.54	1.7
Laitbli	91.72	25.48	2.7
Mainang	91.64	25.56	3.3
Kollong Rock	91.57	25.61	4.4
Suair	91.78	25.42	0.8

[a]The longitudes have been shifted by 0.0417° to the west, correcting a stated error in the station coordinates [*Walker*, 1882].

made up from adjacent stations of each network. These strains are represented by bars whose lengths scale with the magnitude of Γ (equation (3)) and which are aligned with the principal axis of maximum horizontal contraction (equation (4)).

2.1. The Eastern Network of *Bond* [1899]

Oldham [1899] reported the outcome of Bond's measurements as the apparent coseismic displacements of the observation sites and changes in the lengths of lines joining sites (Table 3). *Bond* [1899] derived these quantities from the measured angular changes, defining the orientation and scale of the network by holding fixed the most southerly line, across the Dauki fault. In our earlier study [*Bilham and England*, 2001], in order to remove Bond's assumptions of scale and orientation, we analyzed these data by converting the reported changes in line length and the coseismic displacement vectors back into angle changes. Although Bond's adjustment imposes the minimum number of constraints (origin, scale, and orientation) required to convert angular measurements to displacements, it has the effect of distributing errors throughout the network [*Bibby*, 1982; *Frank*, 1966].

The discovery of a contemporary publication [*Burrard*, 1898] which, in addition to listing line lengths summarized by *Oldham* [1899], also reports Bond's angle changes (Table 1) permits us to refine our analysis of deformation associated with the earthquake. In the southern part of the Shillong Plateau, the angle changes listed by *Burrard* [1898] differ little from those we used in our earlier analysis, but those in the north are sufficiently different to require a revised solution, which we present here. In particular, as can be seen in Figure 1c, changes in the internal angles of the quadrilateral defined by stations 7–9 and 13 were not measured by *Bond* [1899], whereas we [*Bilham and England*, 2001] used changes in these angles that were implied by Bond's adjustment of his observations.

Bond's average closure error for the 1898 survey was 3.41 arcsec, suggesting an average dispersed uncertainty of 1.2 arcsec for each measured angle. *Burrard* [1898] was more conservative in his assessment of errors, asserting that the original triangulation measurements were correct to within 0.3 arcsec and that "Mr Bond's measurements are probably within [2.5 seconds of arc] of the present truth."

2.2. The Assam Valley Network of *Wilson* [1938]

As did Bond, *Wilson* [1938] reported his results as apparent coseismic displacements (Table 2). To convert his angle changes to displacement vectors, he assumed that the extremities of his east-west line at Bharabia and Tatalia (Stations 14 and 35, Table 2) had not moved relative to each other. Some of the 1936 survey angles were subsequently compared with the original 1856 angles by *Nagar et al.* [1989] who were apparently unaware of Wilson's 1938 analysis. *Nagar et al.* [1989, 1992] calculated strain in triangles over a shorter east-west distance between 90.70°E and 91.769°E (between Stations 15 and 28, Table 2), but neither they nor *Wilson* [1938] published Wilson's angle measurements.

Wilson reported a mean triangular error of 0.64 arcsec (3.1 μrad), a high quality that he attributed to the short observing lines between contiguous survey points. Three of the stations were damaged, but the location of their mark stones could be identified with reasonable certainty. The error in the 1856 survey was reported to be 0.3 arcsec, and hence, the combined error was approximately 4 μrad. We estimate that our quantification of *Wilson*'s [1938] plotted displacement vectors introduced azimuthal uncertainties of ±1° and errors in the

lengths of displacement vectors equivalent to ±10 cm. These uncertainties add less than 1 μrad additional uncertainty to the estimated angular error.

We recognize, however, that there may be undetectable errors associated with drafting of the displacement vectors in *Wilson* [1938]. We therefore attempted to test the accuracy of our quantification of Wilson's data by comparing our strain changes with those of *Nagar et al.* [1992] who used (but did not publish) both Wilson's angles and the pre-earthquake angles measured in 1856 [*Walker*, 1882]. This attempt was unsuccessful because we identified a step in Nagar et al.'s procedure that, in our opinion, introduced distortion into the strain analysis whose cause may be diagnosed but whose effect cannot be cured without access to the original angle measurements. Nagar et al. indicate that they carried out a network adjustment for the horizontal displacements of 12 points of their 1856 and 1936 data that allowed only 17 degrees of freedom; this implies three constraints in addition to a minimum of four required to solve for the unknown horizontal displacements. These additional constraints would have distributed errors in displacement gradients throughout the network [*Bibby*, 1982; *Bomford*, 1980] (see also section 2). Unfortunately, Nagar et al. provide no information on the three additional constraints they used. In comparing our estimates of strain with theirs, we find that in some triangles the shear strains agree to within 2 microstrain, but for others they differ by 20 microstrain. A request to the Survey of India to provide Wilson's raw angle observations (in a form comparable to that published by *Burrard*, [1898]) remains unanswered.

2.3. Uncertainties in Triangulation Data

The nominal uncertainties in angle changes for Bond's network are of order 2.5 arcsec (12 μrad), and those for Wilson's observations are smaller. But each set of observations may record displacements that are not directly related to slip in the earthquake. *Bond* [1899] made his measurements at a time when there was still significant aftershock activity which probably caused continuing distortion of the surface, while *Wilson* [1938] made his observations almost 40 years later. In addition, it is probable that some monuments were affected by landsliding, liquefaction, or settling during the earthquake. Accordingly, we adopt a conservative approach, assigning a uniform uncertainty of 3.75 arcsec (18 μrad, a 50% increase over the uncertainty of Bond's measurements) to all the measurements, except for the six additional changes in angles which we have reconstructed from Bond's reports of changes in length of baselines joining sites. Those changes are marked by footnote c in Table 1 and are assigned an uncertainty of 27 μrad because, for these triangles, only two angles were observed so no check on triangle closure was possible.

3. Location and Fault Parameters for the Great 1897 Assam Earthquake

3.1. Analysis of Angle Changes

We model the causative fault of the 1897 earthquake as a rectangular dislocation (with top and bottom horizontal) embedded within a homogeneous elastic half-space [*Okada*, 1992]. In reality, there must be a contrast in rigidity of the near-surface rocks between the sediments of the Brahmaputra plain and the crystalline rocks of the Shillong Plateau. The presence of a low-rigidity near-surface layer causes horizontal surface displacements near the fault to be larger than for a homogeneous half-space [*Cattin et al.*, 1999; *Savage*, 1998]. Accounting for this effect upon the angular changes in the Assam Valley network [*Wilson*, 1938] would require complex physical calculations, the parameters to which (such as sediment thickness and rigidity) are not known with any precision. Furthermore, the sparse available measurements do not warrant a complicated model.

The model has nine free parameters: the horizontal coordinates of each end of the line of intersection between the model fault plane and the free surface, which we refer to as the end points of the model fault; the depths of the top and bottom of the dislocation; its dip; and the strike and dip components of slip on the dislocation. The problem is nonlinear, and, because the observations are sparsely distributed, there are many local minima; it is therefore desirable to seek a global minimum by systematically searching parameter space. In practice this search is seven-dimensional because, with the other parameters fixed, the problem is linear in the components of slip on the plane. Nevertheless, if we were to search through the entire space encompassing the locations that have been proposed for the causative faults of the 1897 earthquake, the computational task would be prohibitive; we therefore adopt a hybrid approach.

We first set a wide bound on our search, allowing the parameters to vary between the limits shown in Table 4. This part of the search is carried out using the downhill simplex minimization of Nelder and Mead [*Press et al.*, 1992]. For each point sampled in parameter space we calculate the displacements for all sites in the

Table 4. Parameters for Slip on the Oldham Fault in 1897[a]

	West End Point		East End Point				Slip	Top	Bottom		
	°E	°N	°E	°N	Dip	Rake	(m)	(km)	(km)	M_w[b]	WRMS
Range	±30 km				15°–75°	-	-	0–20	10–40[c]		
Best fit	90.838	25.910	91.598	25.700	42°	95°	25	6	31	8.19	1.01
Chedrang	90.679	25.901	91.598	25.700	42°	95°	25	6	31	8.24	1.28

[a]The top line shows the range in parameters allowed in the search described in section 3.1. The middle line shows the solution that best fits the geodetic observations. The bottom line shows the solution obtained by augmenting the geodetic observations with information on slip on the Chedrang fault (section 3.2.2).
[b]Calculated from fault area and slip, assuming a shear modulus of 3.3×10^{10} N m^{-2}.
[c]Range of difference in depth between top and bottom of fault.

geodetic networks (Figures 1b and 1c) and compare the angular changes derived from these displacements with those observed (Table 1) or derived from the displacements reported by *Wilson* [1938] (Table 2). To reduce the likelihood of settling on a local minimum, we carry out this procedure with 10,000 independent random choices of starting simplex. The provisional solution is given by the parameter combination that yields the lowest weighted root-mean-square (WRMS) residual, with each residual being weighted by the uncertainties given above (section 2.3).

We then systematically varied the end points of the faults from the provisional solution, over the regions shown in Figure 2 in steps of 1 km, finding the best fitting dip, top, and bottom of the dislocation for each location using the downhill simplex minimization. Finally, we fixed the end points of the model fault plane at their best fitting locations (Table 4) and searched systematically through values of dip, top, and bottom of the fault plane to investigate trade-offs among these parameters. Additionally, in this final step, rake was systematically varied rather than being solved for, as it was in the previous steps.

The parameters of the best fitting solution obtained in this way are listed in Table 4, comparison between the observed and model shear strains in triangles of the observation networks is given in Figure 2, and the comparison between model and observed angle changes is given in Figure 3. Figure 4 shows the trade-offs between dip, rake, and top of the fault plane. We found that variation in the depth of the bottom of the model fault plane had no appreciable influence on the other parameters. Each of the panels of Figure 4 displays a clear minimum in the misfits, but there is a trade-off between depth to the top of the model fault plane and the slip on the plane. The valleys in WRMS in Figures 4a, 4b, and 4d correspond to slip that is buried deeper than 10 km and has a small dextral component (rake ~110°), whereas the best fitting solution has almost pure dip slip.

3.2. Depth Range and Length of Rupture

The depth to the top of the rupture is constrained to be at least 5 km (Figure 4a). The feature of the observations imposing this constraint is the fault-parallel contraction near the projection of the fault to the land surface (Figures 1 and 2); if the fault had reached the surface, then the shear strains there would have shown fault-perpendicular extension. The maximum depth extent of the rupture is constrained only by the observations of angle change toward the southern end of the eastern network (Figure 1b). Solutions that fit almost as well as the best fitting depth of 30 km may be obtained by forcing the bottom of the fault to lie at any depth between 30 and 40 km. However, the principal conclusions of this study are not affected by variability in depth to the base of the rupture.

The eastern intersection of the model fault plane with the surface (eastern end point) is constrained by the large differences in angle changes between the eastern and northern networks, in the neighborhood of this end point (Table 1 and Figures 1b and 2). The location of the western end point is constrained only by the angular changes in the Assam Valley network (Table 2 and Figure 1c), and Figure 2 shows that the fault may be extended beyond its best fitting western end point by over 10 km without significant deterioration of the fit; we discuss this point further in section 3.2.2.

3.2.1. Topographic Data

A location for the fault along the northern edge of the Shillong Plateau is supported by geomorphological evidence. In his report of the Assam earthquake, *Oldham* [1899] argued that the steeply incised gorges on

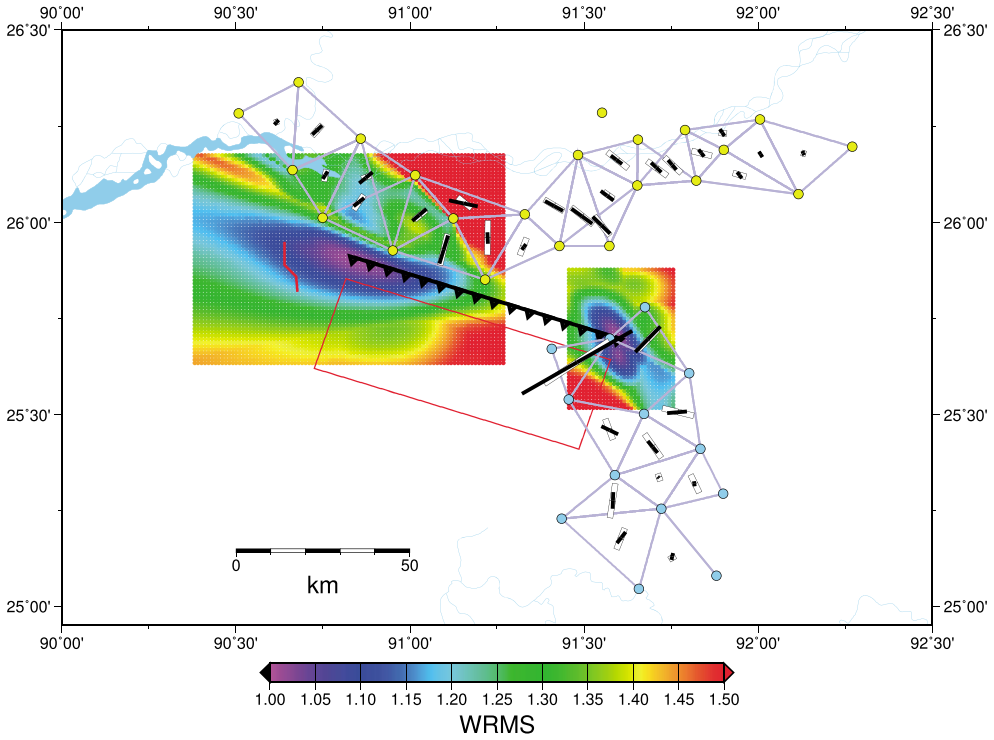

Figure 2. Variation of misfits with locations of the end points of the model fault plane. Colors show the minimum WRMS misfit obtained with the end point at that location and the other parameters allowed to vary. Locations of survey networks as in Figure 1. The intersection between the best fitting fault plane and the level of zero elevation is shown by the black line with teeth; the projection of the model fault plane onto the surface is shown by the red box. Bars, scale to lower left, show the magnitude of Γ (equation (3)) and the orientation of the axis of maximum horizontal contraction (equation (4)). Open symbols correspond to the observations, and black bars correspond to Γs calculated from the best fitting model. In this figure and in Figure 8, goodness of fit for our best fitting model may be evaluated visually by comparing the open rectangle and its direction (observed strain) with the size and direction of the filled black bar (best model prediction).

the northern margin of the plateau mark the location of a reverse fault that causes rapid uplift of the plateau. *Clark and Bilham* [2008] pointed out that the Oldham fault picks out a line of greater steepness of the topography and of north flowing river channels. Here we illustrate Oldham's argument by forming an image of the river valleys from the SRTM data [*Farr et al.*, 2007]. We generate an envelope of the topography by fitting a smooth surface through the highest point in 1×10 km windows, aligned with their long axes parallel to the fault. Subtraction of this smooth envelope from the full topographic data set emphasizes the river valleys (Figure 5a), and we can see, as suggested by *Oldham* [1899] and *Clark and Bilham* [2008], that the intersection of the model fault plane with the surface passes through a line of places where the depths of valleys increase rapidly to the south.

In addition, the profile of the topographic envelope perpendicular to the fault shows a steep northern slope to the plateau with a gentler southward dip across the plateau (Figure 5b). The topographic expressions of the north dipping Dauki and Dapsi faults, which cause tilting to the north, are much less prominent in this longitude range than is that of the Oldham fault. As we discussed in our earlier analysis, it seems likely that the Shillong Plateau is being raised by reverse faulting near both its southern and northern margins [*Bilham and England*, 2001]. There we argued that, if the Dauki and Oldham faults are not to intersect above the base of the seismogenic layer, then they must dip more steeply than about 40° [*Bilham and England*, 2001, Figure 3]; we note, however, that these two faults overlap little in their along-strike directions (Figure 1), so this constraint is not very strong. Similar arguments apply to the relations between the Oldham and Dapsi faults.

Deformation in the plateau may not be restricted to reverse faulting; *Taylor and Yin* [2009] note left-lateral strike-slip faulting to the east of the Oldham fault (Figure 1). The rate of slip on these faults is not known, but their orientation and sense of slip are consistent with their absorbing shortening perpendicular to the reverse faults, with extension E-W along the plateau. Several prominent and linear river valleys within the plateau

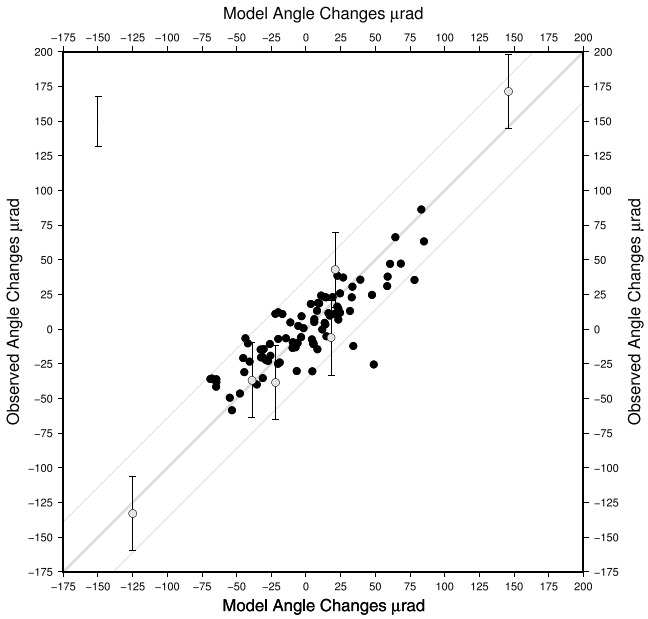

Figure 3. Observed angle changes and angle changes calculated from best fitting fault model. Uncertainties in observations are shown by error bar at top left, except for the six angles reconstructed from Bond's published displacements (Table 1), which are shown by grey symbols with their error bars (section 2.3). Thin grey lines either side of the one-to-one line correspond to misfits of ±36 μrad, equal to twice the uncertainty we assume for the angle changes (section 2.3).

are closely aligned with these faults (Figure 5a), and it may be that further strike-slip faulting remains to be discovered there. Indeed, the 1930 M_w7.1 Dhubri earthquake occurred close to one of these features [*Gee*, 1934] (Figure 5a).

3.2.2. Constraint of Location and Slip of Oldham Fault Using the Observed Slip on the Chedrang Fault

In Appendix A we describe field observations made by *Oldham* [1899] that define the location of and slip upon the Chedrang fault, a ~24 km long down-to-the-west normal fault, which runs approximately perpendicular to the Oldham fault and about 20 km to the west of the western end of the best fitting rupture as defined by the geodetic data. The Chedrang fault slipped by up to 11 m, contemporaneously with the 1897 great earthquake [*Oldham*, 1899]; we suggest that the fault acted as a tear fault that released the concentration of shear stresses on vertical planes at the western end of the rupture of the Oldham fault.

If this suggestion is correct, then we may use Oldham's observations of slip on the Chedrang fault to place constraints on the western end of the main rupture of the 1897 earthquake. We explore these constraints using a boundary element formulation for dislocations in an elastic half-space coded by *Gomberg and Ellis* [1994], after [*Okada*, 1992]. We approximate the Chedrang fault by a set of rectangular panels that follow the complex surface trace of the fault (Appendix A) and whose depths increase to the south, so that their lower edges are consistent with the depth of the Oldham fault (Table 5). We explore the response of these fault segments to displacements on the Oldham fault by finding, for each candidate displacement on the main fault, the distribution of displacements on the separate elements that minimizes the integral of shear stresses over the model Chedrang fault surface.

Uncertainties in the vertical offsets are generally 1 or 2 m, with the exception of the three largest displacements, for which Oldham's measurements permit uncertainties of about half a meter (Table 5 and Figure 6). With the western end point of the Oldham fault fixed to its position derived from the best fit to the geodetic data (Table 4), slip induced on the elements representing the Chedrang fault remains below 20 cm and cannot be significantly increased by changing the depth of the fault elements. With its western end point fixed at this location, slip on the Oldham fault cannot, therefore, explain the observed slip of up to 11 m on the Chedrang fault.

The western end point of rupture on the Oldham fault is not well constrained, however; in particular, Figure 2 shows that misfits to the geodetic data are only slightly degraded if the end point approaches within a few

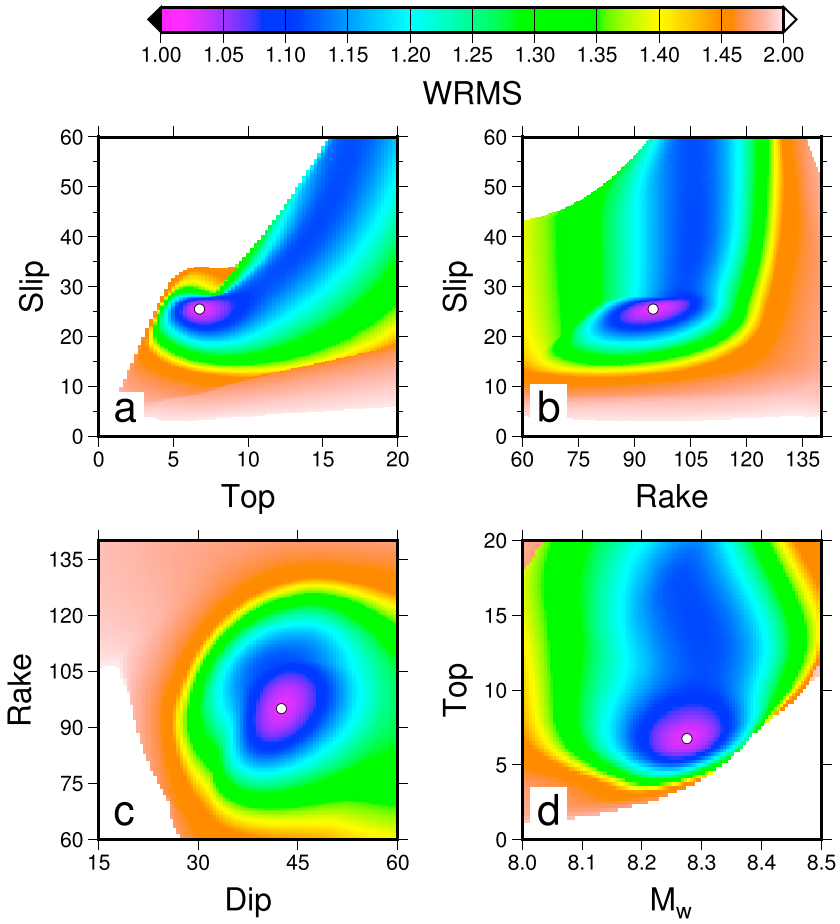

Figure 4. Trade-offs among parameters. End points of the fault are held at the locations given in Table 4, while the other parameters are varied through the ranges shown in Table 4, with rake being allowed to vary between 60° and 140°. Each panel shows the minimum value of the WRMS residual obtained for that two-dimensional slice through parameter space, with white filled circles showing the locations of the minimum misfit. Abrupt cutoffs in Figures 4a, 4b, and 4d reflect the fact that the magnitude of slip is not systematically varied but is obtained as part of the least squares solution (section 3.1).

kilometers of the Chedrang fault. We therefore carried out a grid search, altering the position of the western end point to find the location that generated the best fit to observed slip on the Chedrang fault. In this search the SE end point, the slip, and the dip of the Oldham fault are held constant. For each grid point we calculated maximum slip and the misfit, in a weighted least squares sense, between the calculated and observed slip distribution; the estimated uncertainties in the observations are shown in Table 5.

We find that the locations for the NW end point of the Oldham fault that produce the best fit to slip on the Chedrang fault lie within a small region around 90.74°E, 25.89°N (Figure 6). We do not propose that our calculation offers a definitive solution for slip on the Chedrang fault. We have, for example, assumed uniform slip on the Oldham fault, whereas the real slip distribution in 1897 was presumably much more complex, as is commonly observed in great earthquakes; we have treated the Chedrang fault as being vertical, whereas its dip may shallow with depth, and other complications may readily be imagined.

Given the small number of observations that Oldham made, it is impossible to carry out a detailed analysis of the mechanics of slip on the Chedrang fault. Indeed, the problem is underdetermined because the misfits between calculation and observation may be further reduced by reasonable—though arbitrary—changes to the tops and bottoms of segments of the Chedrang fault. One aspect of Oldham's observations does, however, produce a robust constraint; the slip of over 10 m between 14 and 19 km (Table 5) has an uncertainty of less than 10% of its magnitude. This observation constrains the NW end point of the rupture to lie near 90.74°E,

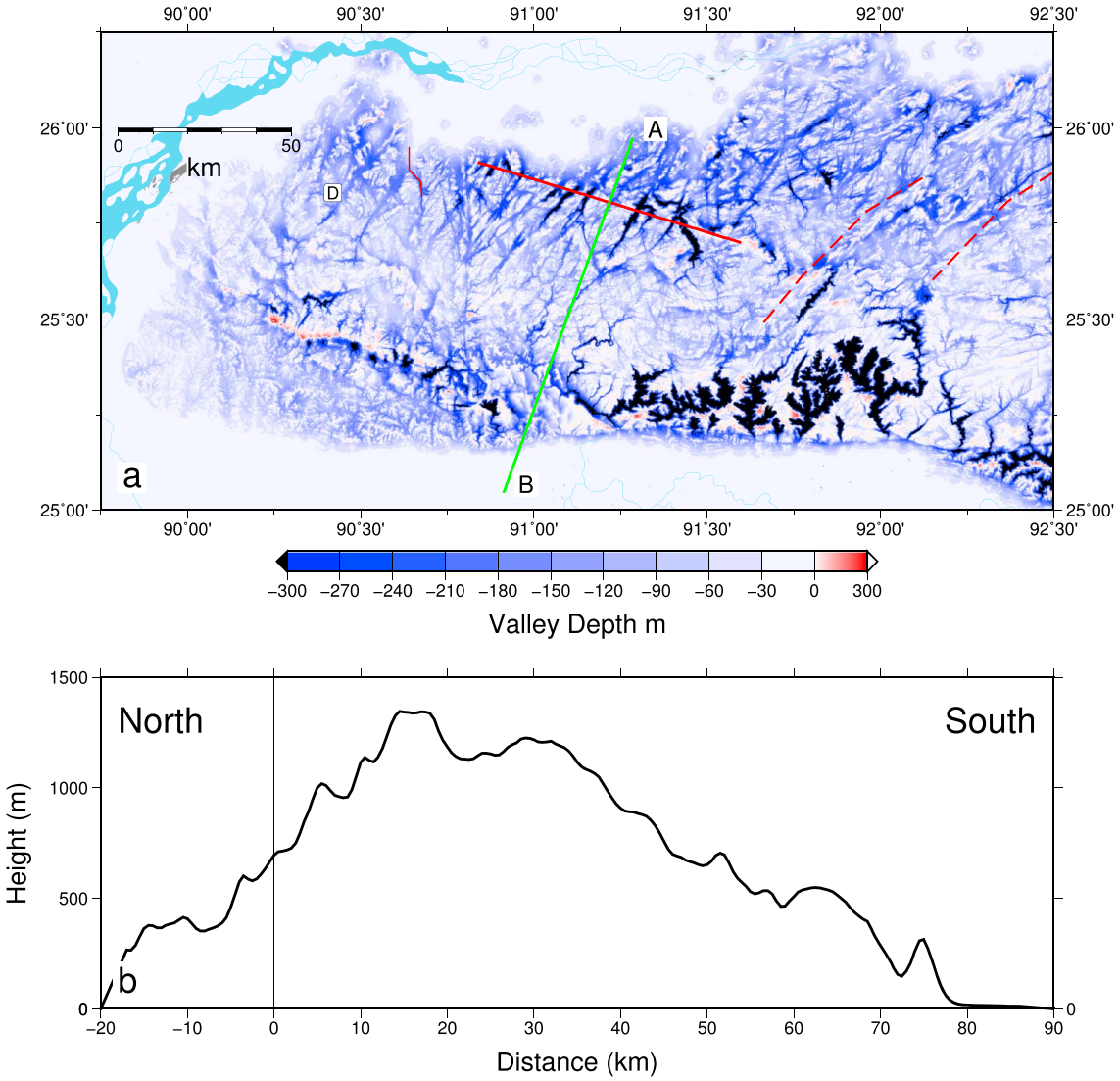

Figure 5. (a) Blue shades show estimates of incision derived from the SRTM DEM [*Farr et al.*, 2007]; see text. Red solid line marks location of best fitting fault; line AB perpendicularly bisects the line of the fault. Dashed lines show the locations given by *Taylor and Yin* [2009] for left-lateral strike-slip faults (see Figure 1). D marks the location of the 1930 M_w7.1 Dhubri earthquake. (b) Profile of the envelope of topography along the line in AB in Figure 5a.

25.89°N (Figure 6), and we regard this location as being the probable end point of the 1897 rupture of the Oldham fault.

4. Discussion

4.1. Fault Parameters of the 1897 Earthquake

The length of the Oldham fault that ruptured was at least 79 km but no longer than 95 km if the argument is accepted that near-synchronous slip of more than 10 m on the Chedrang fault was caused by the stresses generated by the reverse faulting (section 3.2.2). The most unexpected aspect of our solution is that a fault segment which is no longer than 100 km should have experienced slip of 25 m in a single earthquake. This ratio of slip to fault length is at least five times as large as the global average of $2-6\times10^{-5}$ for large intraplate earthquakes [*Scholz et al.*, 1986; *Wells and Coppersmith*, 1994]. Such large slip is required, however, by the magnitudes of the shear strains (Figure 2) and is supported by Bond's observations of uplift by up to 7 m in the hanging wall of the eastern end of the fault (Table 2 and Figure 7). (Recall that the minimum depth of rupture is constrained to be at least 5 km (section 3.2) so that the slip on the fault must be much larger than the observed uplift divided by the sine of the dip.) Our analysis of the motions on the Chedrang fault also support slip of this magnitude near the western end of the rupture (section 3.2.2).

Table 5. Summary of Oldham's Measurements of Vertical Offsets on the Chedrang Fault and Additional Inferences of Offset [a]

Longitude °E	Latitude °N	Depth (km)	Slip (m)	Comment
90.634	26	6	0.5 ± 2	Inferred from *Tandey* [1927]
90.634	25.984	6	4 ± 1.7	Lake depth 5 m
90.633	25.969	6.75	4 ± 1.7	Jhira, *Oldham* [1899]
90.632	25.953	8.25	4 ± 1.7	Estimated from *Oldham* [1899], *Tandey* [1927], and Google Earth map (see Figure A1)
90.631	25.938	9.75	4 ± 1.7	Estimated from *Oldham* [1899], *Tandey* [1927], and Google Earth map (see Figure A1)
90.63	25.922	11.25	4 ± 1.7	Estimated from *Oldham* [1899], *Tandey* [1927], and Google Earth map (see Figure A1)
90.629	25.907	12.75	5 ± 1.4	Estimated from *Oldham* [1899], *Tandey* [1927], and Google Earth map (see Figure A1)
90.638	25.896	14	5 ± 1.4	Estimated from *Oldham* [1899], *Tandey* [1927], and Google Earth map (see Figure A1)
90.647	25.886	14.95	6 ± 1.4	Estimated from *Oldham* [1899], *Tandey* [1927], and Google Earth map (see Figure A1)
90.656	25.876	15.9	10.6 ± 1.4	Estimated from *Oldham* [1899], *Tandey* [1927], and Google Earth map (see Figure A1)
90.665	25.866	16.9	6 ± 1.4	Jolding Wari (sag pond)
90.674	25.856	17.9	6 ± 1	*Oldham* [1899]
90.675	25.846	18.85	11.6 ± 0.5	*Oldham* [1899]
90.676	25.837	19.75	8.3 ± 0.5	*Oldham* [1899]
90.676	25.827	20.7	0.6 ± 1	Two traces (see text)
90.677	25.818	21.85	0.6 ± 0.5	Hillside fractures (see text)
90.677	25.809	22.75	0.3 ± 3	Inferred from Google Earth (Figure A1)

[a]The first three columns show end points and depths of the fault elements used in boundary element modeling of slip on Chedrang fault (section 3.2.2). Each element is a vertical rectangle with surface coordinates given in the nth and $(n+1)$th row of the table (where n is the row number) and with its base at the depth given in the $(n+1)$th row. All elements slip from the surface to the depths shown. Last two columns show estimates of slip on the Chedrang fault at these locations, from *Oldham* [1899], *Tandey* [1927], and Google Earth map (see Figure A1 and text of Appendix A).

Our estimated ratio of 3×10^{-4} for slip to fault length has been approached or exceeded in several other large intracontinental earthquakes, particularly within India. The rupture area of the 2001 Bhuj earthquake is inferred to have been 20 × 20 km with a mean slip of about 10 m, or a slip-to-length ratio of $\sim 5 \times 10^{-4}$. This earthquake occurred on a blind fault that slipped from 35 km to 9 km depth [*Schmidt and Bürgmann*, 2006], in a similar geometry to that we determine for the 1897 earthquake. The 1819 Allah Bund earthquake may have slipped more than 11 m on a 70 km long blind fault—a ratio of $\sim 10^{-4}$ [*Bilham*, 1999], but for this earthquake the subsurface parameters are poorly known. Although they are less secure, because they rely on inferences that observed scarps of prehistorical age were formed in single events, slip-to-length ratios higher than 10^{-4} have also been determined for earthquakes on a 40–50 km section of the Tapti fault [*Copley et al.*, 2014] and on the 35 km long Vijaydurg scarp [*Gaur and Bilham*, 2012]. It seems likely that the long-term slip rates on all these faults are very low so that the slip-to-length ratios may be expected to be higher than for faults with shorter intervals between earthquakes [*Anderson et al.*, 1996].

The minimum estimate of fault length, 79 km, combined with 25 m of slip on a plane whose downdip extent is 37 km (25 km divided by the sine of the dip, Table 4) yields an estimated moment of 2.5×10^{21} N m for the earthquake, or a moment magnitude of 8.19. With the length of 94 km the magnitude becomes 8.24. The principal uncertainties in these estimates arise from the uncertainties in slip (25 ± 5 m) and in the depth of the bottom of the fault (increasing that depth to 40 km would increase the fault length from 37 to 52 km). These considerations decrease the lower bound on the moment to 2×10^{21} N m and raise the upper bound to 4.8×10^{21} N m, giving a range of $8.13 < M_w < 8.4$ for the magnitude of the earthquake, just failing to overlap with the range of $8.0 < M_w < 8.1$ estimated by *Ambraseys and Bilham* [2003] and with the $M_w \sim 8.1$ estimated by *Bilham and England* [2001]. Figure 4d suggests that solutions yielding moments at the extremes of the range involve misfits that are considerably (≳30%) larger than the best fitting solutions. If we restrict the range of acceptable solutions to those whose misfits to the geodetic data are no more than 20% higher than the best fitting solution, then the magnitude range becomes $8.15 < M_w < 8.35$ (Figure 4d).

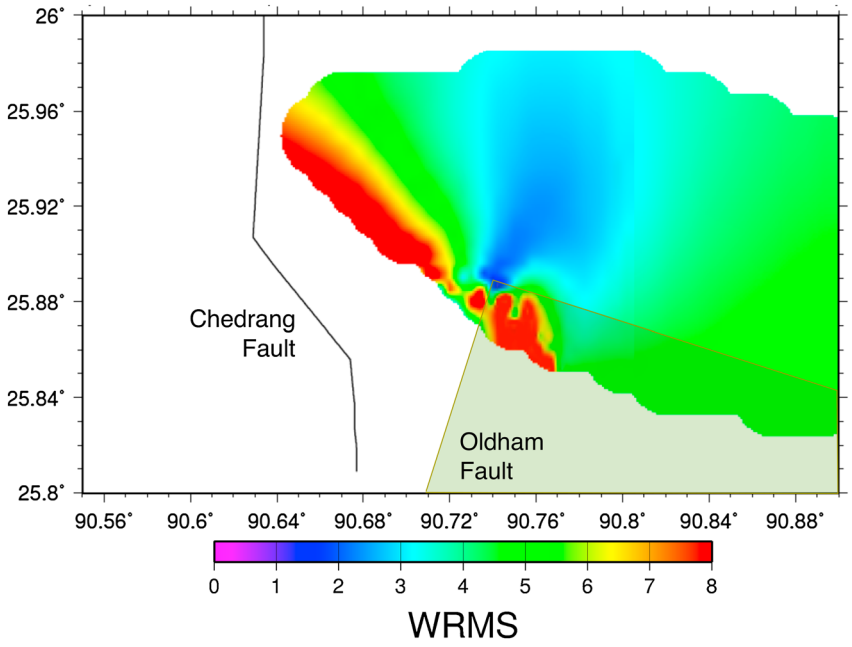

Figure 6. Grid search for optimum location of the NW end point of the Oldham fault. Colors show values of the weighted RMS misfits to observed displacements on the Chedrang for boundary element calculations (section 3.2.2) with the NW end point of the Oldham fault placed at that location. Locations of end points that yield WRMS misfits to the geodetic data (Figure 2) of more than 1.1 (10% worse than the best fitting solution: Figure 2) are excluded.

4.2. Alternative Fault Models

We now address suggestions that the 1897 Assam earthquake occurred on a different fault from the Oldham fault. Several locations have been proposed based on geological, microseismic, seismic intensity, and/or surface deformation data combined with geological and geodetic observations reported by *Oldham* [1899]. The earthquake has been attributed to slip on the Dauki or Dapsi faults [e.g., *Gahalaut and Chander*, 1992; *Kali et al.*, 2012; *Morino et al.*, 2014; *Muhkopadhyay et al.*, 1993] and to slip on a hypothetical fault in the Brahmaputra valley [*Rajendran et al.*, 2004]. These suggestions are, however, incompatible with the geodetic data, as we now demonstrate.

Oldham [1899] initially considered the Dauki fault a viable candidate for the 1897 earthquake, but he changed his opinion because his observations of the severity of observed surface deformation west of 91°E required an epicenter on the north side of the plateau. Oldham's conclusion is clear both in Burrard's report of his discussion with Oldham about design of the triangulation measurements [*Burrard*, 1898] and in Oldham's discussion of the measurements themselves [*Oldham*, 1899, Appendix G]; there is, therefore, no justification for claiming, as do *Morino et al.* [2014], that *Oldham* [1899] attributed the earthquake to slip on the Dauki fault. The geodetic data show that strain decreases from north to south across the Shillong Plateau (Figure 1b) rather than increasing, as would be the case for slip on the Dauki fault (Figures 8a).

Additionally, the greatest uplifts measured by *Bond* [1899] lie at the north of the plateau (Table 2 and Figure 7), rather than at the south, as would be expected for reverse slip on the Dauki fault. We do not use these observations in our solutions because the effects of atmospheric refraction are much more serious on vertical angles than on horizontal ones, particularly when the measurements are taken in a humid environment between stations whose heights differ substantially. Oldham argued for an uncertainty of at least 2 m in height, and the errors would not have been systematic because the vertical angles were measured separately over an interval of several months [*Burrard*, 1898]. Nevertheless, the greatest uplifts observed lie in the region where the greatest uplifts are calculated.

The geodetic solution of *Gahalaut and Chander* [1992] ignored Oldham's triangulation data but used Oldham's observations of subsidence in the Brahmaputra valley to argue for 5 m of oblique reverse slip on a 170 km×100 km patch of the Dauki fault, which they infer to be dipping north at 5°. We attempted to find a model for slip on the Dauki fault that would satisfy the geodetic observations, but, unsurprisingly, all models

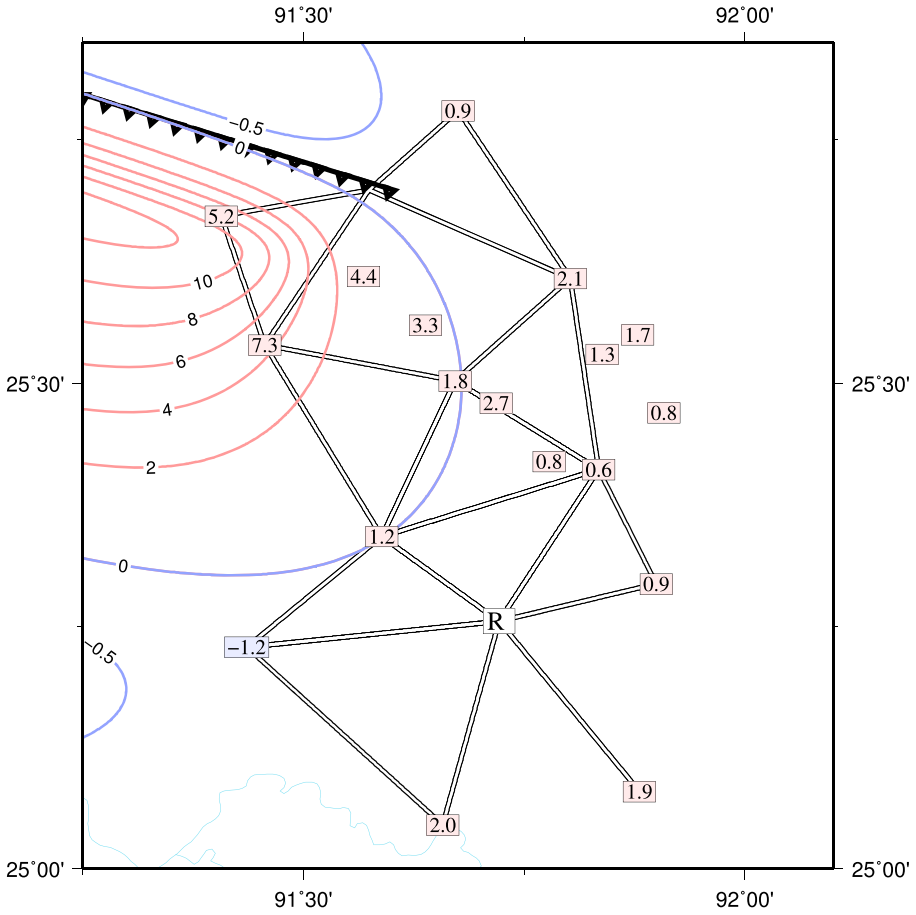

Figure 7. Comparison between observed and calculated surface uplift. Height changes measured by *Bond* [1899] and reported by *Burrard* [1898] and *Oldham* [1899] relative to Rangsanobo (R) (Tables 2 and 3) are shown as symbols in boxes, superimposed on Bond's network. Surface uplift calculated [*Okada*, 1992] from the best fitting fault solution (Figure 2) is shown as colored contours relative to the undeformed Indian plate. All vertical displacements are in meters.

for reverse slip on a north dipping Dauki fault yield surface strain increasing from south to north across the Shillong Plateau rather than decreasing, as observed. Constraining the rake to lie within 15° of 90° [*Gahalaut and Chander*, 1992], we found that the best fitting solution for end points within the regions shown in Figure 8a corresponds to buried reverse slip on a fault dipping at 25°. We note the severe mismatch between observed and predicted shear strains in the north resulting from this solution; the WRMS residuals everywhere within the search region are twice as large as those obtained for slip on the Oldham fault (Figure 2). Better fitting solutions can be found by allowing the end points of the fault to migrate farther from the mapped position of the Dauki fault, but, until the model fault approaches the position of the Oldham fault, the misfits remain unacceptably large.

Equally, the low strain near the Brahmaputra plain and high strain in the northern Shillong Plateau (Figures 1b and 1c) are inconsistent with the suggestion [*Rajendran et al.*, 2004] that the 1897 Assam earthquake occurred on a fault whose projection reaches the surface near the Brahmaputra river (Figure 8b). Again, we searched systematically over end points near the Brahmaputra river, this time finding a best fitting solution with a normal sense of slip. As with the Dauki fault, it is possible to find a local minimum with reverse faulting in the Brahmaputra Valley, as desired by *Rajendran et al.* [2004], but the misfits remain persistently at twice the level obtained for reverse slip on the Oldham fault. Furthermore, had a reverse-faulting earthquake of large slip occurred in this region, it would have resulted in several meters of uplift of the bed of the Brahmaputra precisely where Oldham describes a depression. Additionally, the height changes observed by *Wilson* [1938] (Table 2) and the absence of any substantial change in the course of the Brahmaputra river in 1897 rule out a large dip-slip earthquake in the Valley [see also *Bilham*, 2006].

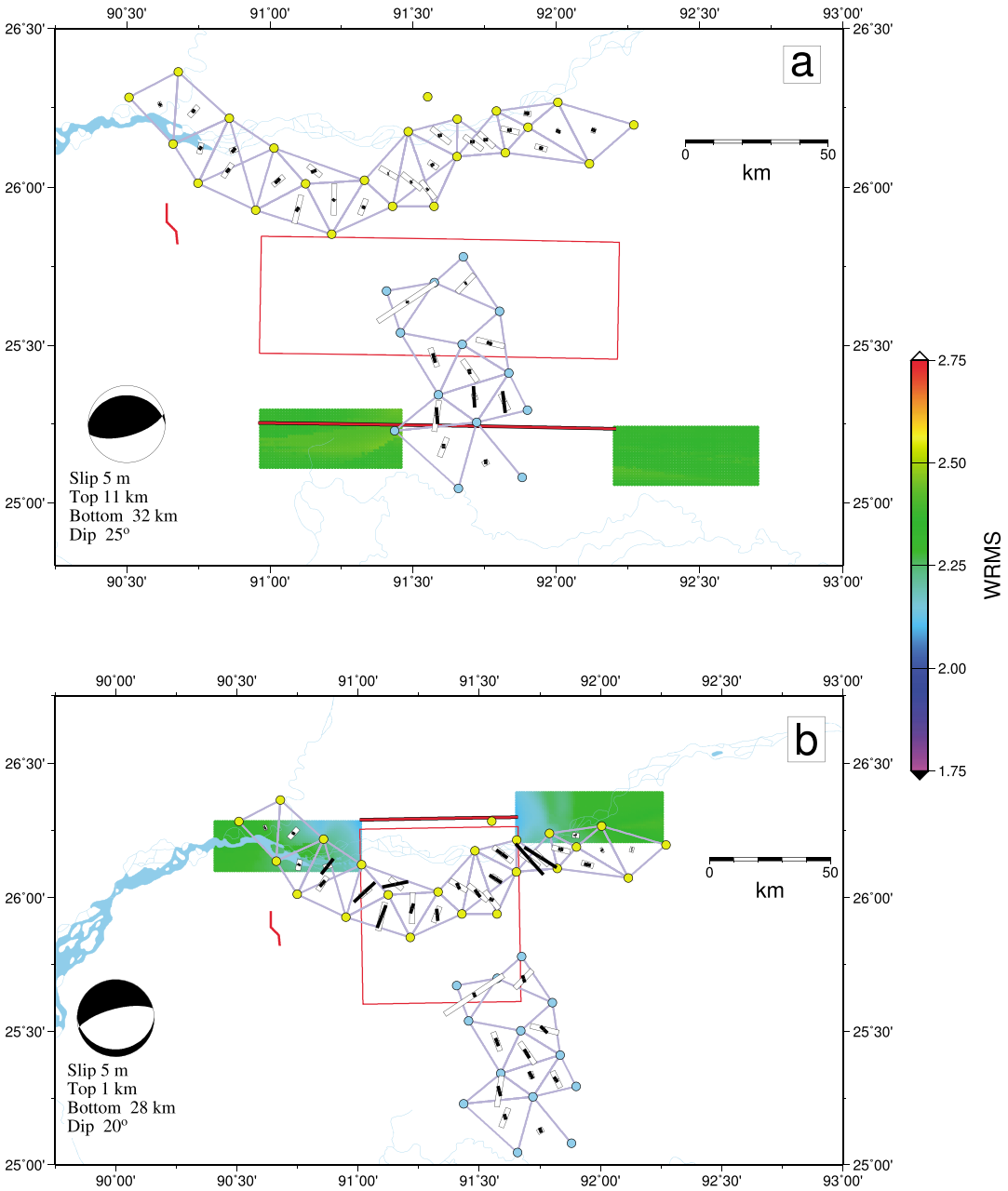

Figure 8. Best fitting solutions to geodetic data obtained for model faults located near the Dauki fault and within the Brahmaputra Valley; symbols as in Figure 2. (a) The results of systematic search for best fitting solutions with end points of the fault constrained to lie close to the Dauki fault. (b) The results of a systematic search covering possible fault locations in the Brahmaputra Valley.

The north dipping Dapsi fault is too far to the west for slip on that fault to have influenced the network of *Bond* [1899]. We do not dispute that the Dauki and Dapsi faults are active; they have clear geomorphic expressions which indicate that they are [e.g., *Ferguson et al.*, 2012; *Kali et al.*, 2013]. Slip on those faults could not, however, account for the geodetic observations made following the 1897 earthquake.

4.3. Implications for Seismic Hazard

GPS observations show convergence between the southern edge of the Shillong Plateau and Bangladesh at approximately 5 mm/yr [*Vernant et al.*, 2014]. If all this convergence were accommodated by earthquakes of the size of the 1897 event (~25 m of slip, equivalent to ~17 m of convergence) the recurrence interval between such earthquakes on individual fault segments would be greater than 3000 years. But the plateau is about

300 km in east-west dimension, while the 1897 earthquake slipped over less than 100 km, so earthquakes must also occur on other fault segments (for instance the Dauki and Dapsi faults) and the recurrence interval between great earthquakes in the whole region must be considerably smaller than 3000 years. It is improbable, however, that the convergence between the southern edge of the Shillong Plateau and Bangladesh is taken up solely by rare great earthquakes, and a more precautionary approach is to assess the hazard posed by smaller but more frequent earthquakes within the volume. We first estimate the time-averaged rate of seismic moment release that would be required to accommodate the strain rate determined by the GPS measurements. For a region of width W, length L, seismogenic thickness S, and shear modulus μ, in which all the strain is released by slip in earthquakes over a time interval t, the elements of the strain rate tensor, $\dot{\varepsilon}_{ij}$, are related to the elements of the summed moment tensor by

$$\Sigma_n M_{ij} = 2\mu t L S W \dot{\varepsilon}_{ij}, \tag{5}$$

where $\Sigma_n M_{ij}$ is the sum of the moment tensors of all n earthquakes taking place in time interval t [*Kostrov*, 1974]. We adopt a length, L, for the plateau of 300 km (~90°E to 93°E, Figure 1) and, based on our analysis here, use a seismogenic thickness, S, of 30 km. We treat the strain as biaxial (shortening perpendicular to the long axis of the plateau, with vertical thickening), so the shortening rate of 5 mm/yr is equal to the across-strike width, W, multiplied by the strain rate. With a value of 3.3×10^{10} N m^{-2} for the shear modulus, we obtain an estimate of $\sim 3 \times 10^{21}$ N m per thousand years for the time-averaged rate of moment release. (We use a thousand years as the time unit, rather than the more usual unit of a year, in recognition of the fact that it makes sense to apply Kostrov's relation only on timescales that are comparable with the recurrence interval of the earthquakes of interest.)

If this rate of moment release is distributed across earthquakes obeying the Gutenberg-Richter relation between magnitude and frequency, then

$$N(M_0) = \alpha M_0^{-\beta}, \tag{6}$$

where N is the number of events having moment greater than or equal to M_0 in a given time interval. M_{tot}, the total moment release over the interval of observation, is

$$M_{\mathrm{tot}} = \int_0^{M_{\mathrm{max}}} M \frac{\mathrm{d}N}{\mathrm{d}\,M}\,\mathrm{d}M = \frac{\alpha\beta M_{\mathrm{max}}^{(1-\beta)}}{1-\beta}, \tag{7}$$

where M_{max} is the maximum scalar moment in the region of interest. We may rearrange equation (7) to yield

$$\alpha = \frac{M_{\mathrm{tot}}\,(1-\beta)}{\beta\, M_{\mathrm{max}}^{(1-\beta)}}. \tag{8}$$

This corrects the expressions (7) and (8) of *Molnar* [1979], which lack the factor β in the numerator of equation (7) and in the denominator of equation (8); we have discussed this correction with Molnar, and he agrees (P. Molnar, personal e-mail communications, 2015).

The value of β is usually found to be about 2/3. Let us assume that the value of M_{max} is approximately the moment of the 1897 event (~3×10^{21} Nm). With this value, and with M_{tot} ~3×10^{21} N m kyr^{-1}, then we estimate that $\alpha \sim 10^{14}$ (N m)$^{\beta}$ kyr^{-1}. The magnitude of α decreases as the one-third power of M_{max} and so would change little if we were to propose, for example, that the maximum earthquake size were an M_0 ~10^{22} N m event, perhaps on the Dauki fault.

With the value of α we calculate, equation (6) leads us to expect one earthquake of the magnitude of the 1897 event every ~2000 years, if the strain rate measured with GPS is all released in earthquakes obeying this moment-frequency relation. Great earthquakes on the borders of the Shillong Plateau must therefore be considered as somewhat less frequent than great Himalayan earthquakes, which appear to have recurrence intervals of 500–1000 years [e.g., *Feldl and Bilham*, 2006; *Bollinger et al.*, 2014]. If this consideration is correct, paleoseismic investigations attributing liquefaction events to great earthquakes on the Oldham fault with recurrence intervals of a few hundreds of years [e.g., *Rastogi et al.*, 1993; *Sukhija et al.*, 1999] must be interpreted with caution. This liquefaction could, however, be associated with smaller, more frequent earthquakes. Our analysis implies that the region would experience three earthquakes of magnitude 7.5 or greater ($M_0 \gtrsim 2 \times 10^{20}$ N m) every thousand years. On average, we should expect one earthquake of magnitude 7 or greater and three of magnitude 6.5 or greater ($M_0 \gtrsim 6 \times 10^{18}$ N m) per century.

Szeliga et al. [2010] identified 10 earthquakes in the region since 1762 that probably had magnitude greater than 6.5 (magnitude estimated from felt intensities using the minimum-magnitude method and allowing for an uncertainty of 0.5 magnitude units). The agreement between observed frequency of damaging earthquakes in the region and that expected from the strain rates estimated from GPS suggests that it would be unwise to concentrate on rare high-magnitude events, such as the 1897 earthquake, in assessing the seismic hazard of the region. Indeed, the 1869 M_w7.4 Cachar earthquake occurred about 200 km to the ESE of the Oldham fault (93.0°N, 25.5°E) [*Oldham*, 1883; *Ambraseys and Douglas*, 2004], and the 1930 M_w7.1 Dhubri earthquake occurred about 50 km to the west of the Oldham and Chedrang faults [*Gee*, 1934]. It will be noted that the city of Shillong (2011 population 143,000, Figure 1) is almost in line with the 1897 rupture and on the same topographic feature. The absence of any known major earthquake between the 1869 and 1897 earthquakes may indicate that the region between the epicenters of these earthquakes, which includes Shillong, is one of high seismic hazard.

5. Conclusions

Reexamination of the geodetic data of *Bond* [1899] and *Wilson* [1938], and geomorphological information, confirms our original conclusion that the great 1897 Assam earthquake took place on a south dipping reverse fault close to the northern edge of the Shillong Plateau [*Bilham and England*, 2001]; we named this fault the Oldham fault. The latitudes of the northeast and northwest end points of the rupture are constrained to within 10 km, ruling out any possibility that the earthquake occurred on a fault near the Brahmaputra river or on the Dauki fault (section 3.2.2 and Figures 2 and 8).

The length of fault that slipped was 79 km, or ~95 km if the displacement of up to 10 m observed by *Oldham* [1899] on the Chedrang fault (Appendix A) is taken into account. The strike of this fault is N110±5°E, subparallel to the Dapsi fault and dipping toward it. The projection of the rupture plane to the surface is marked by steep southward increases both in surface height and in valley depth, consistent with uplift relative to base level of the hanging wall of an active reverse fault (Figure 5). Although comparable geomorphic features are associated with the Dauki and Dapsi faults, slip on those faults cannot account for the observed geodetic deformation (Figure 8).

A remarkable feature of the 1897 earthquake is that, despite ~25 m of reverse slip, coseismic rupture approached no closer than 5 km to the surface (Figure 4). The geodetic evidence requiring blind reverse faulting is the contraction in the region near the projection of the fault to the surface; if slip had reached the surface, then the strain would have been extensional there [e.g. *Segall*, 2010, p 67]. As one might expect for a blind thrust, the geomorphic expression of the Oldham fault is less dramatic than those of the Dauki and Dapsi faults. The earthquake warped the land surface, with $\gtrsim$10 m of relative vertical motion over a distance of 10–20 km (Figure 7), but left few of the clues of seismic activity for which geologists usually search in the epicentral region of major earthquakes. It would, however, be unwise to base assessment of the seismic hazard associated with a fault solely upon the ease with which it can be identified in the field—as several recent devastating earthquakes in the continental interiors have demonstrated [*England and Jackson*, 2011].

Our revised solution suggests that slip on the Oldham fault was greater than we estimated previously (25±5 m rather than 16±10 m). The range of parameters for slip on the rupture corresponds to $8.15<M_w<8.35$ (Figure 4d and section 4.1). Although it is likely that slip at depth in the 1897 earthquake resulted in a reduction in stress within the lower part of the seismogenic crust, stress in the uppermost crust of the northern Shillong Plateau may not have been relaxed, with the implication that seismic hazard may still exist within the region, as has been inferred for smaller blind reverse-faulting events elsewhere [e.g. *Elliott et al.*, 2011, 2013; *Jackson et al.*, 2006].

Appendix A: Oldham's Observations of Faulting Related to the 1897 Earthquake

Oldham visited the epicentral region of the 1897 earthquake in 1898 and reported his observations in his publication on the earthquake [*Oldham*, 1899]. All references to Oldham's observations in this appendix refer to that report. Although Oldham did not observe any features that could be directly attributed to the reverse faulting revealed by the geodetic data, his observations of secondary faulting, particularly of the 24 km long Chedrang fault, provide corroboration of the geodetic solution.

Oldham's name for this fault, which we retain, came from the Chedrang River, now known as the Chidrang River. He observed features such as fault-ponded lakes and fractures whose freshness suggested that the offsets occurred shortly before his traverse of the region. Oldham described vertical slickensides and vertical offsets of up to 11 m that were indicative of pure normal faulting. He also learned that two villagers had been killed during the formation of the largest sag pond near the southern bend of the Chedrang fault (now named Wolding Wari, Table 5) [*Oldham*, 1899, p.142], and because these deaths were believed to have occurred in the main shock, we assume that Chedrang rupture occurred at the same time as the main shock or could have occurred in one of the two large reported aftershocks [*Ambraseys and Bilham*, 2003].

In our earlier analysis [*Bilham and England*, 2001] we envisaged the Chedrang fault to be a straight 20 km long, freely slipping, vertical dislocation extending to depths of ~9 km, stressed by ~16 m of buried reverse slip of the Oldham fault below it and to its east and SE. However, a detailed comparison of Oldham's map with Google Earth scenes taken since 2004 reveals that the surface trace of the fault deviates significantly from a straight line. Here we revise Oldham's map of the fault, and in section 3.2.2 we revise our earlier analysis of the constraints on the location of slip on the Oldham fault that are implied by Oldham's observations of slip on the Chedrang fault. We summarize in Table 5 Oldham's measurements of vertical offsets on the Chedrang fault and our additional inferences of offset, based on his reports and our interpretation of satellite imagery, as discussed below.

Oldham provided no detailed map of the northern half of the fault (north of Dilma, Figure A1), though he described surface flexure of the sediments, and the ponding of lakes relative to various villages to north of Jhira (present-day Zira: elevation ~50 m). The northernmost expression of the fault appears to be close to the low hills NW of Jhira, near where the 5 m deep lake west of Jhira was breached, resulting in the abandonment of the former course of the Krishnai river. Oldham's photograph of the Jhira lake prior to the breach was reproduced by *Marr* [1926], and the depth of the abandoned course of the Krishnai was mapped by *Tandey* [1927] and described briefly by *Nayak* [1985].

Oldham described large fault-ponded lakes near and SE of the confluence of the Krishnai and Chidrang Rivers. The sedimentary deposits across and near the fault have been trenched to a depth of 5 m revealing a possible earthquake dated at 1200 ± 100 years [*Rastogi et al.*, 1993]. Paleoliquefaction of the sediments in the Krishnai valley is reported by *Sukhija et al.* [1999] who find evidence for two or more shaking events, which they propose to have an approximately 500 year return time.

In his account and map of the southern half of the fault from Dilma into the mountains, Oldham refers all features of the Chedrang fault to the Chidrang river. As it flowed downstream to the north the river crisscrossed the fault, alternately damming the river where it flowed eastward into the fault scarp and creating waterfalls where it flowed westward. From his narrative, Oldham's map of his path can be indexed to the Google Earth image (Figure A1a), although, when this is done, we find that the southernmost 4 km of Oldham's map neglects a 30° change in strike and two small lateral offsets that occurred near jogs in the river. One of Oldham's null vertical offsets in the fault occurs at this 30° change in strike, and it is possible that his more southerly null offset is at a relay ramp between two en echelon fractures, but this has not been confirmed by field mapping. In the southernmost 2 km of the fault Oldham noted two parallel fractures separated by 12 m but was unable to follow the fault south of a point where it petered out into a series of hillside fractures at an elevation of around 160 m. South of this point, fault-like features are visible on Google Earth imagery, some of which we show on Figure A1a. We have no evidence that these features were activated in 1897, but the southernmost is quite prominent and may be offset by more than 2 m. Oldham traversed SW to NE across the headwaters of the Chidrang River approximately 10 km south of these points and reported no evidence for southward continuation of the fault. Although he traversed parts of the fault where it crossed hillside spurs along the river valley, where lakes remain ponded to this day (Figure A1b), Oldham describes his map as a "rough plan" and does not claim to have searched hillsides and adjacent valleys for fault offsets.

Oldham describes the length of the Chedrang fault as 12 miles (19.2 km) lost in the alluvium of the Brahmaputra to the north and dying out in thick jungle to the south, with no trace of it in his subsequent SW to NE traverse that passed 8 km south of the region he explored along the river valley. Our remapped fault is similar in length along strike, but we add 1.7 km to its northern end and 3 km to its southern end, to allow for the regions of low slip that Oldham admits may have been missed in the mountains or in the alluvium to the north (Table 5).

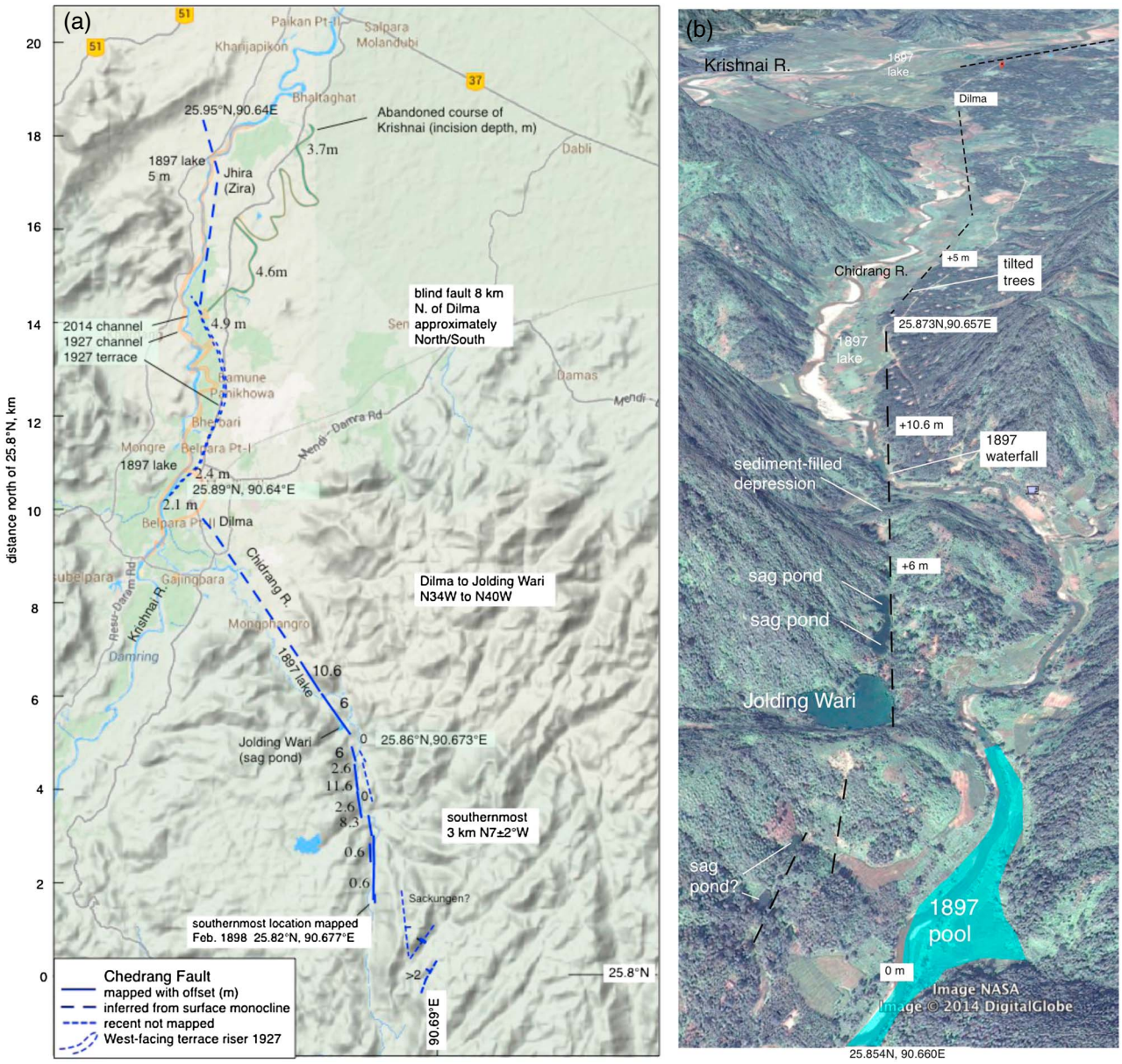

Figure A1. (a) Map of the Chedrang fault constructed from the narrative description given by *Oldham* [1899] and plotted on Google Earth map (2014). Coordinates are given at approximate changes in strike (not noted by Oldham). Former paths of Krishnai river are from *Tandey* [1927] whose map also shows incision depths and the height of a west facing scarp bounding the Dilma/Zira river terrace. (b) Oblique N40W view of Chedrang fault showing features described by *Oldham* [1899]. Indicated slip is up to the NE on vertical slickensides. The foreground pool (now filled with sediments) occurred at a 30° bend in the fault where the projected path of the fault showed no offset. Oldham ascribed the presence of the lake to back tilting of the bed of the stream. The precise path of the fault through the sediments in the distant valley remains conjectural.

Acknowledgments

This work was supported by National Environmental Research Council and the Economic and Social Research Council through grant NE/J02001X/1 to P.E. We thank R. Bürgmann and M. Taylor for helpful reviews. We thank Sujit Dasgupta for drawing our attention to recent geological studies of the Chedrang fault region. R.B. was supported by NSF. The figures were made using GMT [*Wessel and Smith*, 2013]. All the data used in this analysis are given in the tables.

References

Ambraseys, N., and R. Bilham (2003), Reevaluated intensities for the great Assam earthquake of 12 June 1897, Shillong, India, *Bull. Seismol. Soc. Am.*, *93*(2), 655–673.

Ambraseys, N. N., and J. Douglas (2004), Magnitude calibration of north Indian earthquakes, *Geophys. J. Int.*, *159*, 165–206.

Anderson, J., S. Wesnousky, and M. Stirling (1996), Earthquake size as a function of fault slip rate, *Bull. Seismol. Soc. Am.*, *86*(3), 683–690.

Bibby, H. (1982), Unbiased estimate of strain from triangulation data using the method of simultaneous reduction, *Tectonophysics*, *82*, 161–174.

Bilham, R. (1999), Slip parameters for the Rann of Kachchh, India, 16 June 1819, earthquake, quantified from contemporary accounts, in *Coastal Tectonics*, vol. 146, edited by I. S. Stewart and C. Vita-Finzi, pp. 295–319, Geol. Soc. London, Spec. Publ., London.

Bilham, R. (2006), Comment on "Interpreting the style of faulting and paleoseismicity associated with the 1897 Shillong, northeast India, earthquake" by C. P. Rajendran et al., *Tectonics*, *25*, TC2001, doi:10.1029/2005TC001893.

Bilham, R., and P. England (2001), Plateau 'pop-up' in the great 1897 Assam earthquake, *Nature*, *410*(6830), 806–809.

Bollinger, L., S. N. Sapkota, P. Tapponnier, Y. Klinger, M. Rizza, J. V. D. Woerd, D. R. Tiwari, R. Pandey, A. Bitri, and S. B. D. Berc (2014), Estimating the return times of great Himalayan earthquakes in eastern Nepal: Evidence from the Patu and Bardibas strands of the Main Frontal Thrust, *J. Geophys. Res. Solid Earth*, *119*, 7123–7163, doi:10.1002/2014JB010970.

Bomford, G. (1980), *Geodesy*, 4th ed., 855 pp., Oxford Univ. Press, Oxford, U. K.

Bond, J. (1899), Triangulation of the Khasi Hills, in *Annual Report of Triangulation 1897–1898*, edited by C. Strahan, pp. xii–xiii, Survey of India Department, Calcutta, India.

Burrard, S. G. (1898), Report on trigonometrical results of earthquake in Assam, Tech. Rep., Survey of India, Dehra Dun, India.

Cattin, R., P. Briole, H. Lyon-Caen, and P. Pinettes (1999), Effects of superficial layers on coseismic displacements for a dip-slip fault and geophysical implications, *Geophys. J. Int.*, *137*, 149–158.

Clark, M., and R. Bilham (2008), Miocene rise of the Shillong Plateau and the beginning of the end for the Eastern Himalaya, *Earth Planet. Sci. Lett.*, *269*(3–4), 337–351.

Copley, A., S. Mitra, A. Sloan, S. Gaonkar, and K. Reynolds (2014), Active faulting in apparently stable peninsular India: Rift inversion and a Holocene-age great earthquake on the Tapti fault, *Geophys. J. Int.*, *199*, 480–498, doi:10.1093/gji/ggu225.

Elliott, J., A. Copley, R. Holley, K. Scharer, and B. Parsons (2013), The 2011 *Mw* 7.1 Van (eastern Turkey) earthquake, *J. Geophys. Res. Solid Earth*, *118*, 1619–1637, doi:10.1002/jgrb.50117.

Elliott, J. R., B. Parsons, J. A. Jackson, X. Shan, R. A. Sloan, and R. T. Walker (2011), Depth segmentation of the seismogenic continental crust: The 2008 and 2009 Qaidam earthquakes, *Geophys. Res. Lett.*, *38*, L06305, doi:10.1029/2011GL046897.

England, P., and J. A. Jackson (2011), Uncharted seismic risk, *Nat. Geosci.*, *4*, 348–349, doi:10.1038/ngeo1168.

Farr, T., P. Rosen, E. Caro, R. Crippen, R. Duren, S. Hensley, M. Kobrick, M. Paller, E. Rodríguez, and L. Roth (2007), The Shuttle Radar Topography Mission, *Rev. Geophys.*, *45*, RG2004, doi:10.1029/2005RG000183.

Feldl, N., and R. Bilham (2006), Great Himalayan earthquakes and the Tibetan plateau, *Nature*, *444*(7116), 165–170.

Ferguson, E. K., L. Seeber, M. S. Steckler, S. H. Akhter, D. Mondal, and A. Lenhart (2012), The Dauki thrust fault and the Shillong anticline: An incipient plate boundary in NE India?, presented at 2012 Fall Meeting, AGU, San Francisco, Calif., 3–7 Dec Abstract T51F-2665.

Frank, F. (1966), Deduction of earth strains from survey data, *Bull. Seismo. Soc. Am.*, *56*, 35–42.

Gahalaut, V., and R. Chander (1992), A rupture model for the great earthquake of 1897, northeast India, *Tectonophysics*, *204*, 163–174.

Gaur, V., and R. Bilham (2012), Discussion of seismicity near Jaitapur, *Curr. Sci.*, *103*, 1273–1278.

Gee, E. (1934), The Dhubri earthquake of the 3rd July 1930, *Mem. Geol. Surv. India*, *65*, 1–106.

Gomberg, J., and M. Ellis (1994), Topography and tectonics of the central New Madrid seismic zone: Results of numerical experiments using a three-dimensional boundary element program, *J. Geophys. Res.*, *99*(B10), 20,299–20,310.

Jackson, J., et al. (2006), Seismotectonic, rupture process, and earthquake-hazard aspects of the 2003 December 26 Bam, Iran, earthquake, *Geophys. J. Int.*, *166*(3), 1270–1292.

Kali, E., P. Tapponnier, J. van der Woerd, S. Choudhury, S. Baruah, A. K. M. Khorshed Alam, A. Ahsan, C. Dorbath, L. Bollinger, and P. Banerjee (2012), Tectonic geomorphology and active megathrust traces in the East-Himalayan syntaxis, *J. Nepal Geol. Soc.*, *45*, 47.

Kali, E., S. Choudhury, P. Tapponnier, J. van der Woerd, E. A. Okal, L. Bollinger, P. Banerjee, S. Baruah, and A. Coudurier-Curveur (2013), Tectonic geomorphology, aftershock relocation, and sources of the great 1950 and 1897 East Himalayan earthquakes, presented at 2013 Fall Meeting, AGU Abstract T43A-2643.

Kostrov, B. (1974), Seismic moment and energy of earthquakes, and seismic flow of rock, *Izv. Acad. Sci. USSR Phys. Solid Earth*, *97*, 23–44.

Marr, J. E. (1926), *The Scientific Study of Scenery*, 7th ed., 372 pp., London, U. K.

Molnar, P. (1979), Earthquake recurrence intervals and plate tectonics, *Bull. Seismol. Soc. Amer.*, *69*, 115–133.

Morino, M., A. S. M. M. Kamal, S. H. Akhter, M. Z. Rahman, R. M. E. Ali, A. Talukder, M. M. H. Khan, J. Matsuo, and F. Kaneko (2014), A paleo-seismological study of the Dauki fault at Jaflong, Sylhet, Bangladesh: Historical seismic events and an attempted rupture segmentation model, *J. Asian Earth Sci.*, *91*, 218–226, doi:10.1016/j.jseaes.2014.06.002.

Muhkopadhyay, S., R. Chander, and K. N. Khattri (1993), Fine structure of seismotectonics in western Shillong Massif, north east India, *Proc. Indian. Acad. Sci. (Earth Planet. Sci.)*, *102*, 383–398.

Nagar, V. K., A. N. Singh, and A. Prakesh (1989), Strain pattern in N. E. India inferred from geodetic triangulation data, in *Structure and Dynamics of the Indian Lithosphere*, pp. 140–142, India, N. G. R. I. Hyderabad.

Nagar, V. K., A. N. Singh, and A. Prakesh (1992), Strain pattern in N. E. India inferred from geodetic triangulation data, *Mem. Geol. Soc. India*, *23*, 265–273.

Nayak, P. N. (1985), A study of the Chidrang fault and associated structure of the Menghalaya Plateau, *Rec. Geol. Surv. India*, *116*, 75–81.

Okada, Y. (1992), Internal deformation due to shear and tensile faults in a half-space, *Bull. Seismol. Soc. Amer.*, *82*(2), 1018–1040.

Oldham, R. D. (1899), Report on the great earthquake of 12th June 1897, *Memoirs of the Geological Survey of India*, *29*, 1–379.

Oldham, T. (1883), The Cachar earthquake of 10 Jan. 1869, R.D. Oldham (Ed.), *Mem. Geol. Surv. India*, *19*, 1–98.

Press, W., S. Teukolsky, W. Vetterling, and B. Flannery (1992), *Numerical Recipes: The Art of Scientific Computing*, 2nd ed., Cambridge Univ. Press, Cambridge, U. K.

Rajendran, C. P., K. Rajendran, B. P. Duarah, S. Baruah, and A. Earnest (2004), Interpreting the style of faulting and paleoseismicity associated with the 1897 Shillong, northeast India, earthquake: Implications for regional tectonism, *Tectonics*, *23*, TC4009, doi:10.1029/2003TC001605.

Rastogi, B. K., R. K. Chadha, and G. Rajgopalan (1993), Palaeoseismicity studies in Meghalaya, *Curr. Sci.*, *64*, 933–935.

Savage, J. (1998), Displacement field for an edge dislocation in a layered half-space, *J. Geophys. Res.*, *103*(B2), 2439–2446.

Savage, J., and R. Burford (1970), Accumulation of tectonic strain in California, *Bull. Seismol. Soc. Am.*, *60*, 1,877–1,896.

Schmidt, D., and R. Bürgmann (2006), InSAR constraints on the source parameters of the 2001 Bhuj earthquake, *Geophys. Res. Lett.*, *33*, L02315, doi:10.1029/2005GL025109.

Scholz, C., C. Aviles, and S. Wesnousky (1986), Scaling differences between large interplate and intraplate earthquakes, *Bull. Seismol. Soc. Am.*, *76*(1), 65–70.

Seeber, L., and J. G. Armbruster (1981), Great detachment earthquakes along the Himalayan arc and long-term forecasting, in *Earthquake Prediction: An International Review*, edited by M. Ewing, pp. 259–279, AGU, Washington, D. C.

Segall, P. (2010), *Earthquake and Volcano Deformation*, Princeton Univ. Press, Princeton, N. J.

Strahan, G. (1891), Great trigonometrical survey of India, Assam Valley triangulation, Tech. Rep., Survey of India, Calcutta, India.

Sukhija, B., M. Rao, D. Reddy, P. Nagabhushanam, S. Hussain, R. Chadha, and H. Gupta (1999), Timing and return period of major palaeoseismic events in the Shillong Plateau, India, *Tectonophysics*, *308*, 53–65.

Sukhija, B. S., D. V. Reddy, D. Kumar, and P. Nagabhushanam (2006), Comment on "Interpreting the style of faulting and paleoseismicity associated with the 1897 Shillong, northeast India, earthquake: Implications for regional tectonism" by C. P. Rajendran et al., *Tectonics*, *25*, TC2009, doi:10.1029/2005TC001852.

Szeliga, W., S. Hough, S. Martin, and R. Bilham (2010), Intensity, magnitude, location, and attenuation in India for felt earthquakes since 1762, *Bull. Seismol. Soc. Am.*, *100*, 570–584, doi:10.1785/0120080329.

Tandey, E. (1927), Map of Assam: Goalpara District 78K/9, 1:63360, Tech. Rep., Survey of India, Dehra Dun, India.

Taylor, M., and A. Yin (2009), Active structures of the Himalayan-Tibetan orogen and their relationships to earthquake distribution, contemporary strain field, and cenozoic volcanism, *Geosphere*, *5*(3), 199–214.

Vernant, P., R. Bilham, W. Szeliga, D. Drupka, S. Kalita, A. K. Bhattacharyya, V. K. Gaur, P. Pelgay, R. Cattin, and T. Berthet (2014), Clockwise rotation of the Brahmaputra valley relative to India: Tectonic convergence in the eastern Himalaya, Naga Hills, and Shillong Plateau, *J. Geophys. Res. Solid Earth*, *119*, 6558–6571, doi:10.1002/2014JB011196.

Walker, J. T. (1882), The North East Quadrilateral including the Eastern Frontier, Tech. Rep. Ser. Vol. VIII, Great Trigonometrical Survey of India, Dehra Dun, India.

Wells, D., and K. Coppersmith (1994), New empirical relationships among magnitude, rupture length, rupture width, rupture area, and surface displacement, *Bull. Seismol. Soc. Am.*, *84*(4), 974–1002.

Wessel, P., and W. H. F. Smith (2013), Generic mapping tools: Improved version released, *Eos Trans. AGU*, *94*, 409–410, doi:10.1002/2013EO450001.

Wilson, C. A. K. (1938), Triangulation of the Assam Valley Ser., Geodetic Rep., pp. 10–22, Survey of India, Dehra Dun, India.